

Structural, Morphological, Optical and Vibrational Properties of a Novel Coral-Like Fibrous CuO Nanostructure Synthesized via Dropwise Precipitation for UV-light Induced Photocatalytic Wastewater Remediation on Aqueous R6G Dye

Nor Azlia Aziz¹, Chan Kok Sheng^{1,*}, Hui Joo Jie²

¹Faculty of Science and Marine Environment, Universiti Malaysia Terengganu, 21030 Kuala Nerus, Terengganu, Malaysia

²Atomic M&E Sdn Bhd, Jalan Seri Orkid 33, 81300 Skudai, Johor, Malaysia.

ABSTRACT

CuO is a well-known monoclinic structure with unique properties that is extensively investigated for sensor, energy storage, and optoelectronic applications. In this work, the CuO nanostructure was synthesized through facile precipitation by mixing the aqueous copper (II) sulfate pentahydrate with sodium hydroxide. The as-synthesized CuO was characterized by scanning electron microscopy (SEM), X-ray diffractometry (XRD), Fourier transform infrared spectroscopy (FTIR) and UV-visible spectroscopy. A homogeneous growth of a narrow, fine coral-like fibrous morphology was observed on CuO under SEM imaging. The FTIR spectra reveal the existence of some dominant sharp bands in the lower wavenumber region that represent the Cu-O bonds. The high solubility of CuO in water confirms the formation of particles with nanoscale dimensions. CuO exhibits a strong optical absorption peak at 510 nm, and the band gap determined by Tauc's relation is 2.11 eV. CuO is capable of inducing photocatalytic degradation on R6G dye solutions under low-intensity UVC irradiation, which can serve as a future photocatalyst for wastewater treatment.

Keywords: CuO nanostructure; dropwise precipitation; optical properties, R6G dyes, photocatalytic degradation

1. INTRODUCTION

Recently, metal oxide nanostructured materials with dimensions less than 100 nm have acquired tremendous concern and research interest from the scientific community because of their outstanding physical and chemical properties in many invaluable scientific and technological applications. Impressively, tenorite p-type copper oxide (CuO) semiconductors with a monoclinic phase have emerged as one of the most promising transition metal oxides due to their narrow optical band gap in the range of 1.20–1.80 eV. This band gap is tunable by modifying the morphology and size of the nanostructure [1-4]. In addition, CuO also has the advantages of high structural stability, intense optical absorption, eco-friendliness, harmlessness, low cost, and natural abundance accompanied by superior optical, thermal, and electrical properties, which is broadly utilized in superconductors, sensors, detectors, optoelectronic and energy storage devices, heterogeneous catalysis, water purification, and other biomedical applications. Henceforward, it has become increasingly important to fabricate a superior CuO nanostructure by applying suitable synthesis methods, which can contribute to improved structural morphology and optical properties [5-8].

* Corresponding author: chankoksheng@umt.edu.my

Previously, several physical and chemical synthesis techniques have been used to formulate various forms of CuO morphologies (nanocubes, nanotubes, nanoparticles, nanospheres, nanoflakes, nanosheets, and nanorods), such as hydrothermal, green-mediated, sol-gel, sonication, spray pyrolysis, precipitation, and microwave-assisted irradiation methods [9-13]. However, there still exists the synthetic methods with high production costs, low product yield, and even low crystallinity. Facile precipitation is well established as one of the most efficacious, inexpensive, rapid, and environment-friendly wet chemical techniques. Beneficially, this technique needs only a low reaction temperature to accurately modify the size and structure, which is also applicable for mass production [13-15]. In this work, the CuO nanostructures were synthesized via a precipitation method by mixing the aqueous copper (II) sulfate pentahydrate with sodium hydroxide. The crystalline structure, functional groups, optical properties, and surface morphology of CuO samples were characterized by XRD, FTIR, SEM, and UV-Vis spectrophotometry. Subsequently, the photocatalytic degradation activity of these materials was further evaluated towards R6G dye solution under UV light irradiation, which has not yet been reported by other researchers. By referring to previously reported works [2, 4, 7, 16, 17], researchers mainly focused on the photocatalytic performance of CuO under visible light. Alternatively, low-power, high-energy UV light at a cost comparable to visible light, as conducted in this study, could be considered for photocatalytic applications in the near future.

2. MATERIALS AND METHODS

The starting materials used were copper (II) sulfate pentahydrate ($\text{CuSO}_4 \cdot 5\text{H}_2\text{O}$) and sodium hydroxide (NaOH), both procured from Merck Ltd. These raw materials were of analytical grade and used directly without any special treatment. In the beginning, a solution of $\text{CuSO}_4 \cdot 5\text{H}_2\text{O}$ at a concentration of 0.2 M was heated under vigorous stirring. When the solution temperature reached 70 °C, 1.0 M NaOH was added dropwise to the solution until the formation of a brown precipitate at the bottom of the solution, which indicates the formation of CuO at the recorded pH of 12. The precipitate was collected through filtration after the solution was cooled to room temperature. This precipitate was repeatedly washed with distilled water to remove the unwanted impurities and further dried in the air for 6 hours. Finally, the powder was collected and stored in a desiccator for further characterization.

The surface morphology of the as-synthesized CuO samples was characterized by a scanning electron microscopy (SEM, Tescan Vega) at an accelerating voltage of 15 kV. The crystallinity and structure of CuO nanostructures were analyzed from X-ray diffraction patterns obtained from an X-ray diffractometer (Rigaku Miniflex II), where the scanning range was set between $2\theta = 10^\circ - 80^\circ$ with a $\text{CuK}\alpha$ radiation source ($\lambda = 1.54059$). The optical absorbance spectra were recorded using a UV-visible spectrophotometer (Shimadzu, Japan). The photocatalytic activity of CuO was investigated for the color degradation of R6G dye under UV light irradiation. As a first step, a solution of R6G dye was prepared at a concentration of 5 ppm (5 mg/l). Thereafter, 30 mg of CuO was added to 100 ml of dye solution, and the aqueous mixture was stirred in the dark for 30 minutes to achieve an adsorption-desorption equilibrium state. Next, this mixed solution was placed in an enclosed, dark box and emitted with UV light at various time intervals, up to 180 minutes. A small amount of the solution under illumination was collected every 20 minutes to allow the absorbance spectra to be recorded using the UV-Vis spectrophotometer. The fading of dye color or decrease in dye concentration against time can be monitored through a reduction in the absorbance peak intensity of the R6G dye centered at 526 nm.

3. RESULTS AND DISCUSSION

3.1 Morphological Analysis

SEM analysis was performed to examine the surface morphology of the sample. Figures 1(a) and 1(b) exhibit the SEM micrographs of the CuO nanostructures at two different magnifications of $\times 10,000$ and $\times 15,000$, respectively. As observed from the figure, the overall surface morphology of the sample is uniform, whereas many small nanoparticles agglomerate to form a larger coral-like nanostructure that acts as a solid base. Furthermore, we can see from the figure that many fine fibers outgrow the surface of the aggregated nanoparticles. These fibers have very small diameters ranging from 30 nm to 120 nm and lengths varying between 190 nm and 480 nm, as measured by ImageJ software. The average diameter and length are calculated to be 70.66 nm and 346 nm, respectively. Each fiber can be constructed from many small nanocrystallites surrounded by grain boundaries [18-20]. The size distributions of the diameter and length of the coral-like fibrous CuO nanostructure are displayed as the histograms in Figures 2(a) and 2(b), respectively. Normally, the smaller size obtained, especially in the nanosize domain, can increase the surface area and grain boundaries, which in turn allows the material to serve as an effective photocatalyst to stimulate the charge carrier transition between the valence and conduction bands [21-23].

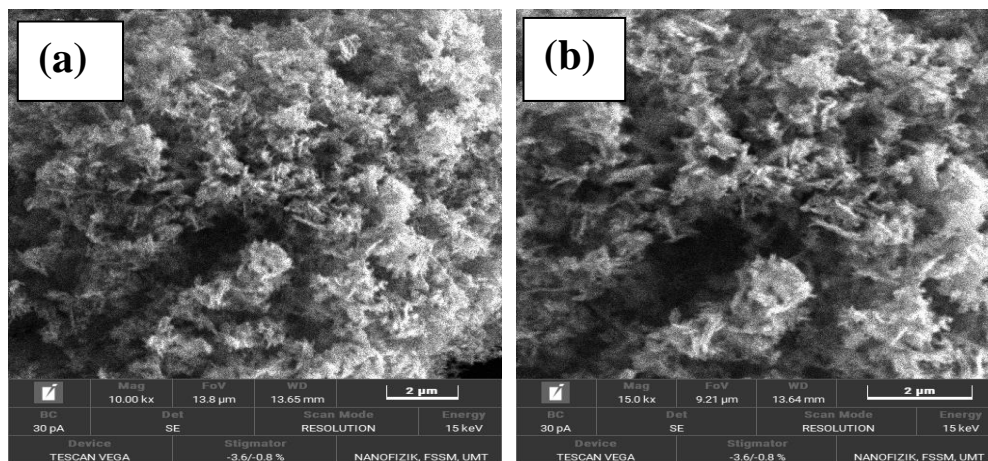


Figure 1. SEM image of as-prepared coral-like CuO nanostructure with magnifications of (a) $\times 10,000$ and $\times 15,000$.

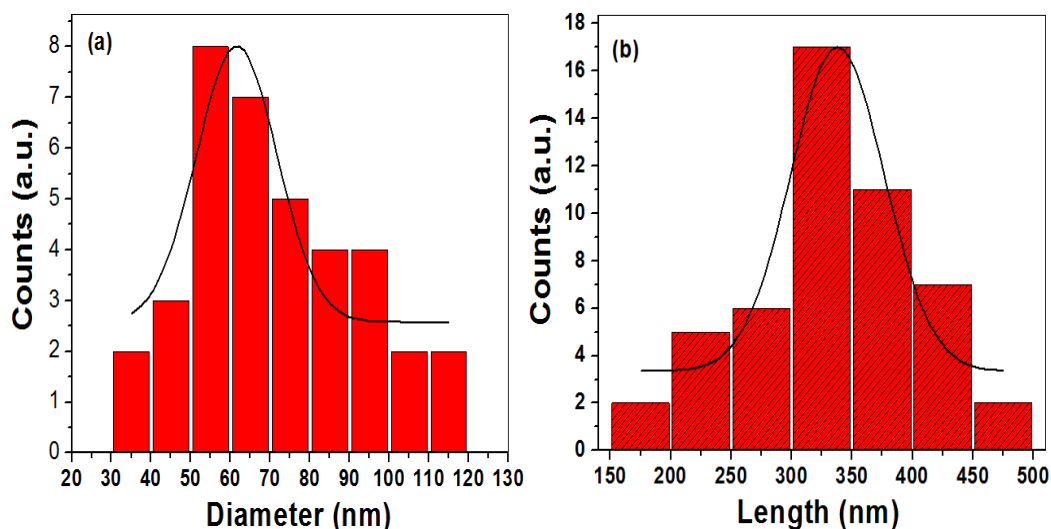


Figure 2. Size distribution histograms of CuO for the: (a) diameter (b) length of coral-like fibrous nanostructure.

3.2 Crystalline structure

XRD measurements were performed to determine the crystal structure of the studied material. Figure 1 presents the XRD pattern visible in the 2θ range for the present CuO nanostructures. As shown in the figure, CuO is a single polycrystalline material without exhibiting any amorphous characteristics. Furthermore, the peaks located at 32.46° , 35.62° , 38.63° , 48.85° , 53.61° , 58.19° , 61.39° , 66.33° , 68.20° , 72.40° and 75.08° correspond respectively to the following planes: (1 1 0), (0 0 2), (1 1 1), (-2 0 2), (0 2 0), (2 0 2), (-1 1 3), (-3 1 1), (2 2 0), (3 1 1) and (0 0 4), by matching well with the JCPDS card no. 00-48-1548 for a monoclinic structure of the C2/c symmetry space group. Gudipati *et al.* [16] and Pavithra *et al.* [17] also found the same CuO structure as obtained in this study, whereby the techniques they each used were biogenically and combustion synthesis, respectively. Moreover, sharp and dominant peaks with narrow bandwidths can be observed at $2\theta = 35.50^\circ$, 35.65° and 38.63° , which implies that CuO has relatively high crystallinity in the respective planes. No other peaks related to impurities or other sub-compounds such as Cu (OH)₂ and Cu₂O were traced through XRD, indicating a very high phase purity of CuO [24-26].

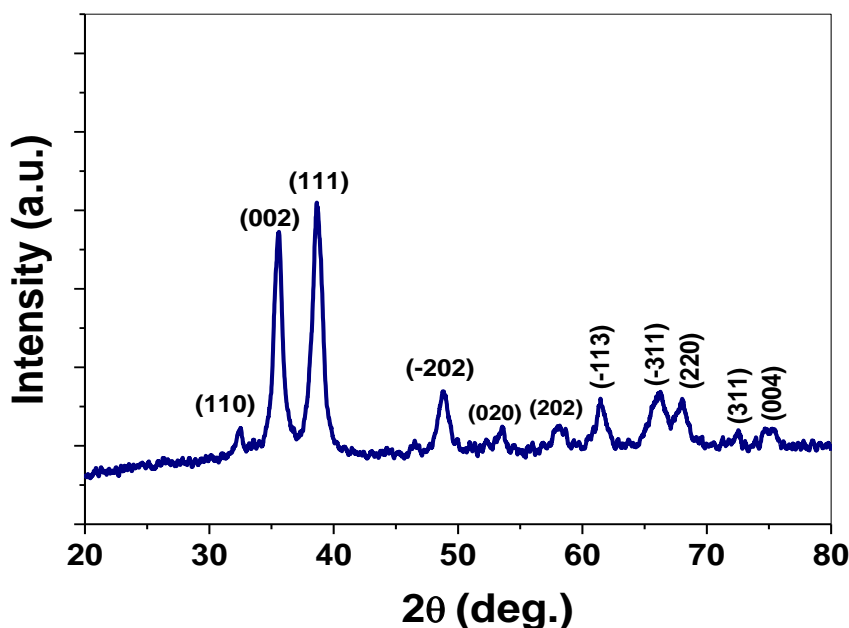


Figure 3. XRD pattern of CuO nanostructure.

3.3 Optical Properties

The optical absorption properties were characterized at room temperature by the UV-visible spectrophotometer. Figure 4(a) displays the optical absorption spectra of the CuO nanostructure in the 400–800 nm wavelength range. As can be seen from the figure, the CuO demonstrates an intense absorption peak at 510 nm. Such a finding suggests that CuO, with its very fine nanostructure, has improved hydrophilicity and hence allows this material to be readily dissolved in water. Another possible reason for this phenomenon can be due to the

presence of many O-H bonds that are attached to the surface of molecules, as evidenced by the FTIR spectra analysis. Henceforward, the band gap is accessed according to Tauc's formula as follows [27-30]:

$$(\alpha h\nu) = B(h\nu - E_g)^{1/2} \quad (1)$$

where α denotes the optical absorption coefficient, h symbolizes Planck's constant, ν represents the radiation frequency, B is a proportionality constant, E_g stands for band gap energy and n indicates the types of electronic transition. Herein, because CdS is a semiconductor material with a direct band gap, n is assigned a value of 1/2 corresponding to this property. The plot of $(\alpha h\nu)^2$ against photon energy for the present CuO samples is displayed in Figure 5. To obtain the band gap energy, a straight line is fitted to the linear portion of the curve in the higher energy region, where the point that this line intersects at the photon energy axis denotes the band gap value. By referring to the value indicated in the figure, the band gap determined for CuO is 2.11 eV, a value larger than the literature band gap of bulk CuO, which lies between (1.2-1.8) eV [31-35]. This result further suggests that photons with higher energy are required to initiate the charge carrier transitions when comparing the CuO nanostructure with bulk CuO. Advantageously, a larger band gap can reduce the recombination rate between electrons and holes and further impoverish the effectiveness of photocatalytic reactions [37-39]. From the work reported by Peng et al. [31], it was found that the widening of the band gap can be achieved through the reduction of crystallite size.

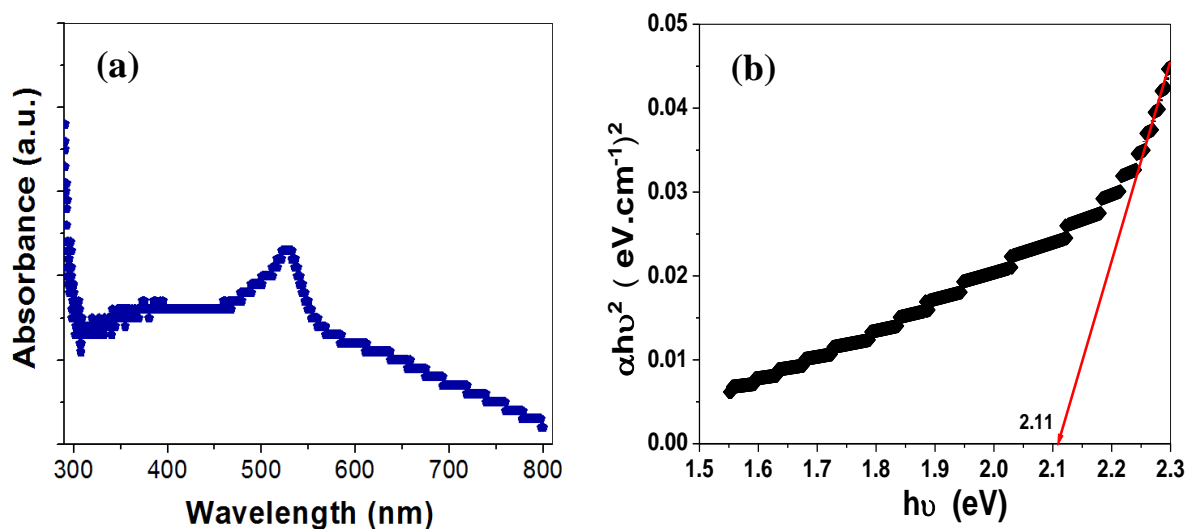


Figure 4. (a) UV-Vis optical absorption spectra and (b) $(\alpha h\nu)^2$ versus photon energy of the CuO sample.

3.4 Functional Groups

The FTIR spectra of CuO nanostructure that were recorded within the range of 4000-400 cm^{-1} are illustrated in Figure 5. The occurrence of functional groups in the investigated materials is represented by the vibrational band positions in the spectrum. From the figure, it can be clearly seen that a broad band is located around 3429 cm^{-1} , indicating the hydroxyl (O-H) stretching vibration due to the absorption of atmospheric water molecules on the sample surface [40, 41]. On the other hand, a sharp peak observed at 1742 cm^{-1} is attributed to the H-O-H bending vibration [42-44]. Meanwhile, a strong, sharp peak emerged at 2360 cm^{-1} mainly corresponds to the CO_2 molecules that attached to the surface of CuO nanostructures during synthesis [22]. In

addition, the small peaks that are positioned at 1367 cm^{-1} , 1221 cm^{-1} , 1113 cm^{-1} and 918 cm^{-1} can be assigned to stretching vibrations of C-O, C-C, C=O and C-H deformation, respectively [21, 23, 24]. Notably, some other sharp and prominent bands appeared ranging from 540 cm^{-1} to 650 cm^{-1} , which reflects the Cu-O molecular bonding [11, 20, 21].

3.5 Photocatalytic degradation on R6G dye

Subsequently, the resulting CuO was utilized as a photocatalyst to study the color bleaching effect on R6G dye solution under UV illumination as a model pollutant for the remediation of sewage. The change in the absorption spectrum against the irradiation time is illustrated in Figure 6(a). As demonstrated in the figure, the dominant peak observed at 526 nm is due to the absorbance of the R6G dye solution, and this peak gradually decreases with the prolongation of UV irradiation time. A discernible reduction in the absorption peak intensity indicates that the UV light has successfully stimulated the color fading of the aqueous R6G dye, where this dye has been reported to have high photostability and is commonly used in the manufacturing of textiles and optical filters in dye lasers [41]. Figure 6(b) depicts the plot of degradation percentage as a function of irradiation time. From the result, it is found that the dye degradation percentage

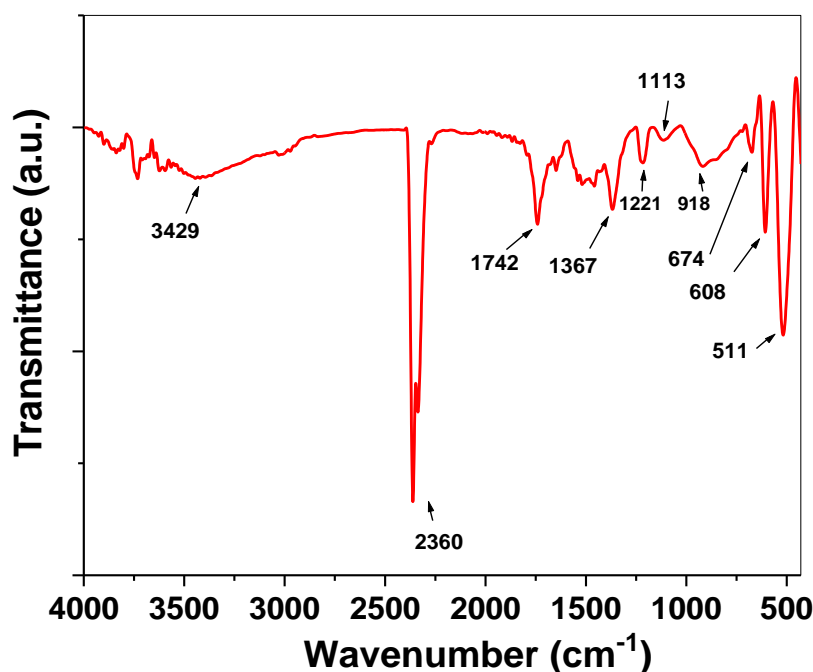


Figure 5. FTIR spectra of as-prepared coral-like fibrous CuO nanostructure.

risks with a longer UV exposure time. Initially, the degradation percentage increases gradually over the first 60 minutes, which indicates that the dye photodecolorization takes place at a slower rate. Thereafter, a steeper slope can be observed from the plot, which can be attributed to a rapid dye degradation rate until the entire irradiation time is completed. This finding indicates that the combination of UV and CuO is effective in stimulating the degradation of R6G dye in an aqueous solution over a prolonged period of time. The relations of C/C_0 and $\ln(C/C_0)$ versus the irradiation time are plotted as given in Figures 6(c) and 6(d), respectively. Hence, a linear relationship can be observed from the fitted line to the experimental data, as indicated in the plot of $\ln(C/C_0)$ versus irradiation time. This result validates that the photocatalytic degradation activity of CuO towards R6G dye complies with the law of pseudo first-order reaction kinetics given by Equation 2 [3, 8, 41]:

$$\ln\left(\frac{C}{C_0}\right) = -kt \quad (2)$$

where C_0 represents the original aqueous dye concentration, C designates the dye concentration at any time intervals of time, t and k is the 1st order kinetic rate constant. The rate constant value obtained from the gradient of the fitted line is $1.3852 \times 10^{-4} \text{ min}^{-1}$ with a high correlation coefficient value of $R = 0.9283$. The computed kinetic parameters prove that the use of CuO nanostructures as photocatalysts can render active centers for the photobleaching of R6G dyes since the dye decomposition is insignificant without the presence of catalysts. For further explanation, the dye degradation effect is due to the generation and separation of electron-hole pairs in the catalyst, which is caused by the absorption of sufficient UV photon energy by the electrons to overcome the band gap barrier, and in turn transfer to a higher energy level [16, 21]. In this study, when the CuO catalyst was irradiated with UV light, the photon energy of this light was absorbed by the catalyst and resulted in the generation of electron-hole pairs. The electron-hole pairs then reacted with O_2 and H_2O to originate the free radicals that consequently degraded the R6G dye molecules into non-toxic components [2, 3, 8, 21]. As reported by Harun et al. [45], the degradation efficiency can be enhanced by applying a higher quantity of photocatalyst or increasing the UV light power [45-47].

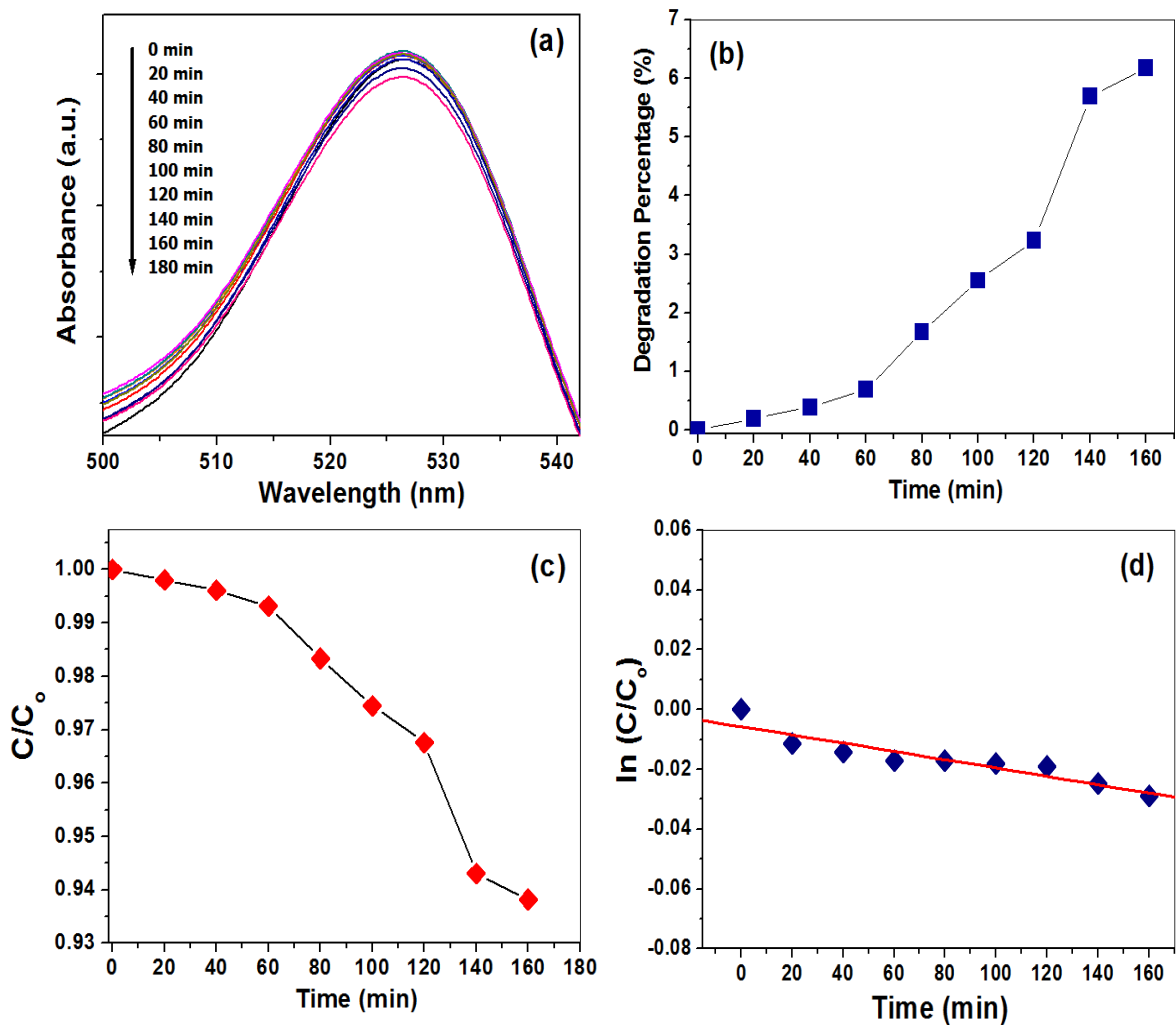


Figure 6. (a) Variation of absorption spectra of R6G under UV irradiation; (b) percentage of degradation with irradiation time; (c) degradation curve of C/C_0 and (d) first-order kinetics fitting on

$\ln(C/C_0)$ versus exposure time for R6G degradation.

5. CONCLUSION

In summary, CuO nanostructures were successfully formulated via dropwise precipitation by mixing the copper (II) sulfate pentahydrate and sodium hydroxide in an aqueous solution. SEM images reveal a formation of very fine coral-like fibrous nanostructures with small fiber diameters determined as low as 30 nm. Several prominent peaks located in the low wavenumber range in the FTIR spectra indicate the existence of Cu-O bonding. CuO shows a major absorption peak at 510 nm and a band gap of 2.11 eV is determined from the Tauc's relation. CuO was also utilized as a photocatalyst to induce the degradation of R6G dye under weak UV light, which can potentially serve as future wastewater treatment.

ACKNOWLEDGEMENTS

The authors gratefully acknowledge the Universiti Malaysia Terengganu and the Malaysian Government for this work's technical and financial support through the research grant (UMT/TAPE-RG/2020/55290).

REFERENCES

- [1] Q. Zhou, Y. Zhang, T. Zeng, Q. Wan, N. Yang, *Anal. Chim. Acta* 1171, 338663 (2021).
- [2] A. George, D. M. A. Raj, X. Venci, A. D. Raj, A. A. Irudayaraj, R. L. Josephine, S. J. Sundaram, A. M. Al-Mohaimed, D. A. A. Farraj, T. Chen, K. Kaviyarasu, *Environ. Res.* 203, 111880 (2022).
- [3] A. Ahmad, M. Khan, S. Khan, R. Luque, K. M. Abualnaja, O. K. Alduaij, T. A. Yousef, *J. Mol. Struct.* 1256, 132522 (2022).
- [4] A. George, D. M. A. Raj, A. D. Raj, B. Nguyen, T. Phan, T. Pazhanivel, K. Sivashanmugan, R. L. Josephine, A. A. Irudayaraj, J. Arumugam, V. Nguyen, *Mater. Lett.* 281, 128603 (2020).
- [5] N.A. Aziz, C.K. Sheng, *Rom. J. Phys.* 68, 610 (2023).
- [6] Z. Yang, Q. Rong, T. Bao, M. Jiao, L. Mao, X. Xue, W. Wen, Z. Wu, X. Zhang, S. Wang, *Anal. Chim. Acta* 1199, 339598 (2022).
- [7] A. K. Sibhatu, G. K. Weldegebrieral, S. Sagadevan, N. N. Tran, V. Hessel, *Chemosphere* 300, 134623 (2022).
- [8] K. Alsamhary, N. M. Al-Enazi, E. Alhomaidi, S. Alwakeel, *Environ. Res.* 207, 112172 (2022).
- [9] H. J. Prabu, R. Varghese, I. Johnson, S. J. Sundaram, A. D. Raj, R. Rajagopal, P. Kuppusamy, R. Sathya, K. Kaviyarasu, *Environ. Res.* 212, 113295 (2022).
- [10] A. P. M. Udayan and S. N. Sawant, *J Phys Chem Solids* 150, 109883 (2021).
- [11] N. A. S. K. Anuar and C. K. Sheng, *J. Nano- Electron. Phys.* 13, 05015 (2021).
- [12] U. Nakate, Y. Yu and S. Park, *Microelectron. Eng.* 251, 111662 (2022).
- [13] Z. R. Parekh, S. H. Chaki, A. B. Hirpara, G. H. Patel, R. M. Kannaujiya, A. J. Khimani and M. P. Deshpande, *Physica B Condens. Matter.* 610, 412950 (2021).
- [14] C. K. Sheng and Y. M. Alrababah, *Kuwait J. Sci.* 49, 1-10 (2022).
- [15] C. K. Sheng and Y. M. Alrababah, *J. Nano- Electron. Phys.* 12, 01017 (2020).
- [16] T. Gudipati, M. B. Zaman, P. Singh and R. Poolla, *Inorg. Chem. Commun.* 130, 108677 (2021).
- [17] N. S. Pavithra, K. N. Manukumar, R. Viswanatha and G. Nagaraju, *Inorg. Chem. Commun.* 130, 108689 (2021).
- [18] Y. M. Alrababah, C. K. Sheng and M. F. Hassan, *Nano-Struct. Nano-Objects* 19, 10034 (2019).
- [19] K. S. Chan and W. M. M. Yunus, *Pertanika J. Sci. Technol.* 13, 23-30 (2005).

- [20] A. George, D. M. A. Raj, A. D. Raj, A. A. Irudayaraj, J. Arumugam, M. S. kumar, H. J. Prabu, S. J. Sundaram, N. A. Al-Dhabi, M. V. Arasu, M. Maaza and K. Kaviyarasu, *Surf. Interfaces* 21, 100761 (2020).
- [21] A. G. Raju, B. D. Rao, G. Himabindu and S. M. Botsa, *J. Mater. Res. Technol.* 17, 2648-2656 (2022).
- [22] M. An, L. Li, X. Gao, Y. Zhu, J. Guan and Q. Wu, *Colloids Surf. A: Physicochem. Eng. Asp.* 643, 128794 (2022).
- [23] N. S. Pavithra, K. N. Manukumar, R. Viswanatha and G. Nagaraju, *Inorg. Chem. Commun.* 130, 108689 (2021).
- [24] D. Das and P. Nandi, *Appl. Surf. Sci.* 570, 151260 (2021).
- [25] Q. Qin, N. Qiao, Y. Liu and X. Wu, *Appl. Surf. Sci.* 521, 146479 (2020).
- [26] G. Wang, Y. Zhang, L. Ge, Z. Liu, X. Zhu, S. Yang, P. Jin, X. Zeng and X. Zhang, *J. Hazard. Mater.* 429, 128282 (2022).
- [27] N.A. Aziz, C.K. Sheng, *Dig. J. Nanomater. Biostructures* 18, 203-210 (2023).
- [28] K. Sahu, B. Satpati and S. Mohapatra, *Ceram. Int.* 46, 24407-24412 (2020).
- [29] C. K. Sheng, K. A. M. Amin, L. L. Hong, M. F. Hassan and M. Ismail, *Int. J. Electrochem. Sci.* 12, 10023-10031 (2017).
- [30] Y. M Alrababah, C. K. Sheng and M. F. Hassan, *Chalcogenide Lett.* 16, 297-301 (2019).
- [31] W. Peng, Y. Zhou, J. Li, Y. Liu, J. Zhang, G. Xiang, X. Zhu, R. Li, H. Wang and Y. Zhao, *Mater. Sci. Semicond. Process.* 131, 105883 (2021).
- [32] N. S. Pavithra, K. N. Manukumar, R. Viswanatha and G. Nagaraju, *Inorg. Chem. Commun.* 130, 108689(2021).
- [33] S. Kulkarni and R. Ghosh, *Sens. Actuators B Chem.* 335, 129701 (2021).
- [34] A. Ghosha, M. Miahb, A. Beraa, S. K. Sahab and B. Ghosha, *J. Alloys Compd.* 862, 158549 (2021).
- [35] H. Absike, Z. Essalhi, H. Labrim, B. Hartiti, N. Baaalla, M. Tahiri, B. Jaber and H. Ez zahraouy, *Opt. Mater.* 118, 111224 (2021).
- [36] J. Uddin, M. Sharmin, M. N. Hasan and J. Podder, *Opt. Mater.* 119, 111388 (2021).
- [37] S. Sharma, K. Kumar, N. Thakur, S. Chauhan and M. S. Chauhan, *J. Environ. Chem. Eng.* 9, 105395 (2021).
- [38] B. Uma, K. S. Anantharaju, L. Renuka, S. Malini, S. S. More, Y.S. Vidya and S. Meena, *Ceram. Int.* 47, 10355-10369 (2021).
- [39] M. F. A. Aziz, N. L. A. Wahab and K. S. Chan, *Mal. J. Microsc.* 7, 109-115 (2011).
- [40] W. M. M. Yunus, K. S. Chan and W. M. Z. W. Yunus, *J. Nonlinear Opt. Phys. Mater.* 12, 91 100 (2003).
- [41] M. F. Hassan, S. K. Zainuddin, K. H. Kamarudin, C. K. Sheng, M. A. A. Abdullah, *Malaysian J. Anal. Sci.* 22, 238-248 (2018).
- [42] N. Jamsuzazilawati, C. K. Sheng, W. M. Z. Yunus, *Jordan J. Phys.* 15, 377-381 (2022).
- [43] C. K. Sheng, W.M.M. Yunus, W. Md. Z. W. Yunus, M. Z. Ab. Rahman, *Mater. Phys. Mech.* 48, 1-8 (2022).
- [44] C. K. Sheng, D. M. Fong, *J. Eng. Sci. Technol.* 17, 4107-4116 (2022).
- [45] N. Harun, C. K. Sheng, M. G. M. Sabri, A. N. Dagang, H. Salleh, *J. Optoelectron. Biomed. Mater.* 12, 9-15 (2020).
- [46] M. E. Bustos, F. Hevia, S. Fuentes, A. I. Martínez, R. A. Zárate, *Mater. Lett.* 297, 129936 (2021).
- [47] G. Sabeena, S. Rajadurai, E. Pushpalakshmi, H. A. Alhadlaq, R. Mohan, G. Annadurai and A. Maqusood, *J. King Saud Univ. Sci.* 34, 102092 (2022).

